# Electronic Structure of Luminescent $d^0$ Niobium and Tantalum Imido Compounds *cis,mer*-$M(NR)Cl_3L_2$

**Darryl S. Williams*,‡ and Andrey V. Korolev**

Contribution from Department of Chemistry, 145, Wayne State University, Detroit, Michigan 48202

*Received January 22, 1998*

Electronic absorption and emission spectra are reported for luminescent $d^0$ monoimido group 5 compounds $M(NR)Cl_3L_2$ (M = Nb, Ta; R = alkyl, aryl; L = dme, $Cl^-$, py). These compounds display weak ($\epsilon < 200\ M^{-1}\ cm^{-1}$), well-resolved lowest-energy transitions in the high-energy visible and near-UV regions ($20\,000 < E_{abs} < 29\,000\ cm^{-1}$). The energy of this absorption band depends strongly on the nature of the imido substituent, with a significant decrease observed when aryl groups are present. Excitation into this transition results in long-lived luminescent excited states. Long emission lifetimes (50 ns to 17 $\mu$s) and high quantum yields (0.001−0.24) are observed, decreasing primarily as a function of the alkyl substituent, being lowest in the aryl imidos. Good overlap is observed with absorption, excitation, and emission mirror spectra, indicating absorption into and emission from the same excited state. The data are consistent with absorption into and emission from a $^3$(nb, $\pi$) state, or $d_{xy} \leftarrow$ Ta−N $\pi$. Semiempirical molecular orbital calculations are presented which suggest that the imido compounds may be considered as having highly mixed but localized Ta═N $\pi$-bonding. A significant difference is noted in $[Ta(NPh)Cl_5]^{2-}$, in which there is appreciable aryl character in Ta═N $\pi$-type orbitals. This accounts for the difference in electronic properties of the aryl imidos compared to the alkyl imidos. An analysis of radiative and nonradiative excited-state deactivation pathways is presented. Significantly, an energy gap law correlation is observed for nonradiative decay in the imido compounds as a group, but a corresponding correlation of radiative rates with emission energy is not observed when aryl and alkyl imidos are compared, evidence of electronic perturbation by the aryl substituent.

## Introduction

The explosion in early transition metal chemistry of compounds containing multiply bonded ligands (MBLs) and, in particular, imido ligands, during the last twenty years or so is evidence of the great utility and unusual reactivity of organometallic compounds relying on $\pi$-bonding to saturate the valence shell of the central atom.[1−4] Imido ligands ($NR^{2-}$) in particular are highly stabilizing ancillary ligands, enhancing the stability of low-coordinate, electronically unsaturated molecules.[4,5] The alkyl substituent provides good solubility in nonpolar solvents and (variable) steric protection of the metal center from oligomerization reactions. Imidos are generally considered good electronic models for the ubiquitous oxo ligand,[1−4] which suffers from a tendency to bridge between unsaturated metal centers and is acknowledged to be a weaker $\pi$-donor.[1] Early preparations of imido compounds relied on alkyl/aryl isocyanates or imines, but preparations now afford imidos in high yield from the amine, base, and metal oxide or halide, for nearly any organic substituent one may desire.[6] Syntheses of well-defined, mononuclear imidos from readily available starting materials have been reported for most of the metals in groups 4−8.[4]

There are a number of studies, at varying levels of theory, considering the electronic structures of imido[7−9] and other compounds containing MBLs;[10] however, experimental investigations remain rare.[11−28] We wish to understand the electronic

* To whom correspondence should be addressed.

‡ Current address: Texas Eastman Division, Eastman Chemical Company, P.O. Box 7444, Longview, TX 75607-7444,

(1) Nugent, W. A.; Mayer, J. M. *Metal−Ligand Multiple Bonds*; Wiley: New York, 1988.
(2) Collman, J. P.; Hegedus, L. S.; Norton, J. R.; Finke, R. G. *Principles and Applications of Organotransition Metal Chemistry*; University Science Books: Mill Valley, CA, 1987.
(3) Cotton, F. A.; Wilkinson, G. *Advanced Inorganic Chemistry*, 5th ed.; John Wiley & Sons: New York, 1988.
(4) Wigley, D. E. *Prog. Inorg. Chem.* **1994**, *42*, 239−482.
(5) Gibson, V. C. *J. Chem. Soc., Dalton Trans.* **1994**, 1607−1618.
(6) Korolev, A. V.; Rheingold, A. L.; Williams, D. S. *Inorg. Chem.* **1997**, *36*, 2647−2655.
(7) Benson, M. T.; Bryan, J. C.; Burrell, A. K.; Cundari, T. R. *Inorg. Chem.* **1995**, *34*, 2348−2355.
(8) Cundari, T. R.; Conry, R. R.; Spaltenstein, E.; Critchlow, S. C.; Hall, K. A.; Tahmassebi, S. K.; Mayer, J. M. *Organometallics* **1994**, *13*, 322−331.
(9) Schofield, M. H.; Kee, T. P.; Anhaus, J. T.; Schrock, R. R.; Johnson, K. H.; Davis, W. M. *Inorg. Chem.* **1991**, *30*, 3595.
(10) Neuhaus, A.; Veldkamp, A.; Frenking, G. *Inorg. Chem.* **1994**, *33*, 5278−5286.
(11) Korolev, A. V.; Williams, D. S. Manuscript in preparation.
(12) Williams, D. S.; Thompson, D. W.; Korolev, A. V. *J. Am. Chem. Soc.* **1996**, *118*, 6526−6527.
(13) Brewer, J. C. Synthesis, Characterization, and Reactivity of trans-Dioxorhenium(V) and -(VI) Complexes. Ph.D. Thesis, California Institute of Technology, Pasadena, CA, 1991.
(14) Che, C.-M.; Lau, T.-C.; Lam, H.-W.; Poon, C.-K. *J. Chem. Soc., Chem. Commun.* **1989**, 114−116.
(15) Cowman, C. D.; Trogler, W. C.; Mann, K. R.; Poon, C. K.; Gray, H. B. *Inorg. Chem.* **1976**, *15*, 1747.
(16) Heinselman, K. S.; Hopkins, M. D. *J. Am. Chem. Soc.* **1995**, *117*, 12340−12341.
(17) Heinselman, K. S.; Miskowski, V. M.; Geib, S. J.; Wang, L. C.; Hopkins, M. D. *Inorg. Chem.* **1997**, *36*, 5530−5538.
(18) Hopkins, M. D.; Miskowski, V. M.; Gray, H. B. *J. Am. Chem. Soc.* **1986**, *108*, 6908−6911.
(19) Lam, H.-W.; Che, C.-M.; Wong, K.-Y. *J. Chem. Soc., Dalton Trans.* **1992**, 1411−1416.
(20) Manna, J.; Gilbert, T. M.; Dallinger, R. F.; Geib, S. J.; Hopkins, M. D. *J. Am. Chem. Soc.* **1992**, *114*, 5870.
(21) Neyhart, G. A.; Seward, K. J.; Boaz, J.; Sullivan, B. P. *Inorg. Chem.* **1991**, *30*, 4486−4488.

S0020-1669(98)00074-3 CCC: $15.00 
Published on Web 07/03/1998

structure of these species from an experimental standpoint and relate it in a practical way to a relatively simple theoretical model. A crystal field model would consider the imido as a soft[29] chloride analogue. An MO treatment provides a more accurate picture, determined by the accuracy of the basis set and level of theory, which can range from complex to incomprehensible[10] depending on symmetry and the other ligands in the compound. Somewhere between the extremes is a mental picture which is pedagogically accurate but simple enough to understand and without unnecessary detail. Relatively complex interactions can be understood with simple models, as Hoffmann showed using extended Hückel theory in his series of papers on various fragments of inorganic and organometallic species.[30−34] Similarly, we wish to connect a relatively simple MO picture with electronic spectroscopic results in a straightforward manner which, while rigorous, is not overly complex.

There are now a few examples of $d^2$ compounds containing MBLs which luminesce in fluid solution at room temperature, including dioxo,[13,25−28] nitrido,[14,18,19,21,35] and alkylidyne[20,36] species. The formally LF (ligand field)[15,18] excited states are long-lived, displaying proton- and electron-transfer reactivity.[19,35] A very few $d^0$ compounds containing MBLs have been reported as luminescent, including $Cp^*_2ScCl$,[23] $Cp^*TaCl_3L$ (L = Cl, $RCO_2$, $RSO_3$),[22] $M(N)(OR)_3$ (M = Mo, W; solid state),[24] and $Ta(NR)X_3L_2$.[12,16] These observations are very exciting from the inorganic photochemist's viewpoint in that $d^0$ compounds containing one MBL seem to represent a new class of luminescent inorganic chromophore.

## Results

**Coordination Environment.** A recent report details the synthesis of a wide variety of $Ta(NR)Cl_3L_2$ compounds including incorporation of any alkyl substituent[37] at the imido position, including those reported here.[6] These compounds are pseudooctahedral with a cis,mer geometry about tantalum, as is clear from NMR and crystallographic data.[12,16,17,38] The Nb═N bond length in $Nb(NCMe_3)Cl_3(dme)$[6] is completely normal for $d^0$ group 5 imido compounds,[4] as is that for $[Nb(NCMe_3)Cl_4(py)]^-$,[39] $Ta(NAr)Cl_3(dme)$,[17] $[Ta(NAr)Cl_5]^{2-}$ (Ar = 2,6-$^i$Pr$_2$−C$_6$H$_3$),[40] or $Ta(NPh)Cl_3(PEt_3)(THF)$.[41] From a structural perspective, these compounds represent a useful series due to the consistent geometry as R, M, and L are varied. Lack of significant competition from the ligand set with the imido ligand for $\pi$-type orbitals on the metal center is assumed. The numbering scheme for these compounds includes an arabic number for each imido alkyl substituent followed by a letter corresponding to the identity of L (**a**, L = py; **b**, L = $Cl^-$; **c**, L = 1/2 dme).[6]

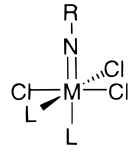


M = Nb, Ta

R = Alkyl, Aryl

L = 1/2 dme, $Cl^-$, py

**Absorption Spectra.** The diamagnetic compounds $Ta(NR)Cl_3L_2$ exhibit weak absorption bands in the visible region when R is aryl and in the near-UV region when R is an alkyl group. Spectral band maxima and molar absorptivities are concentration independent and are listed in Table 1. Typical spectra are presented in Figure 1. In each case, the lowest-energy absorption (labeled Band I) is well-resolved from intense higher-energy bands in the UV portion of the spectrum (Band II) of the aryl imidos and high-energy tails (Band III) which appear at the solvent limit (~240 nm).[12,16] Absorption maxima for Band I range from 20 900−28 700 $cm^{-1}$ with molar absorptivities from 73 to 180 $M^{-1}$ $cm^{-1}$ (±10%) in the tantalum imidos. Similar trends are noted for the niobium compounds, which have lower absorption energies and lower molar absorptivities (30−60 $M^{-1}$ $cm^{-1}$) compared to the tantalum compounds. Band I is nearly Gaussian in shape ($\Delta\bar{\nu}_{1/2} \sim 5000$ $cm^{-1}$) and appears to consist of a single transition. In the cyanophenyl (**10**) and anthryl (**12**) imido compounds, this transition is more broad, tailing into Band II and further into the low-energy portion of the visible region. This results in these compounds appearing more tan in color than other aryl imidos, which range from red-orange ($Ta(NAr)Cl_3py_2$) to yellow ($Ta(N\text{-}4\text{-}CN\text{-}C_6H_4)Cl_3(dme)$). The alkyl imido compounds are pale yellow (py adducts) or white (dme adducts). Absorption maxima and molar absorptivities for Band I do not change appreciably in different solvents, as observed for $Ta(N^tA)Cl_3(dme)$ in 1,2-dce, $CH_2Cl_2$, toluene, or $Et_2O$. In each case, $\lambda_{max}$= 343(2) nm (29 200 $cm^{-1}$) and $\epsilon$ = 160(10) $M^{-1}$ $cm^{-1}$.

Band I maxima vary over a range of about 8000 $cm^{-1}$ (~1 eV) for these compounds as the imido substituent and Lewis base ligands are varied. Changing L from an ether to pyridine lowers the absorption energy by 1000−1500 $cm^{-1}$. The difference in energy of Band I between n-Bu ($E_{abs}$ (**6c**) = 29 200 $cm^{-1}$) and 2,6-$^i$Pr$_2$−C$_6$H$_3$ ($E_{abs}$ (**8c**) = 22 500 $cm^{-1}$), however, is 6700 $cm^{-1}$; thus there is a significant effect on the electronic structure of these compounds from the aryl substituent.[12] By comparison, changing X from Me to Ph in $Re(4,4'\text{-}X_2\text{-}bpy)(CO)_3Cl$ lowers the MLCT absorption by only 1500 $cm^{-1}$.[42] One might also compare this change with that observed in $(1,10\text{-phen})Re(CO)_3Cl$ ($\lambda_{max}$ = 38 000 $cm^{-1}$) and (4,7-Ph$_2$-1,10-

(22) Paulson, S.; Sullivan, B. P.; Caspar, J. V. *J. Am. Chem. Soc.* **1992**, *114*, 6906.
(23) Pfennig, B. W.; Thompson, M. E.; Bocarsly, A. B. *Organometallics* **1993**, *12*, 649−655.
(24) Pollagi, T. P.; Stoner, T. C.; Dallinger, R. F.; Gilbert, T. M.; Hopkins, M. D. *J. Am. Chem. Soc.* **1991**, *113*, 703−704.
(25) Thorp, H. H.; Van Houten, J.; Gray, H. B. *Inorg. Chem.* **1989**, *28*, 889−892.
(26) Thorp, H. H.; Kumar, C. V.; Turro, N. J.; Gray, H. B. *J. Am. Chem. Soc.* **1989**, *111*, 4364−4368.
(27) Winkler, J. R.; Gray, H. B. *J. Am. Chem. Soc.* **1983**, *105*, 1373−1374.
(28) Winkler, J. R.; Gray, H. B. *Inorg. Chem.* **1985**, *24*, 346−355.
(29) Pearson, R. G. *J. Am. Chem. Soc.* **1963**, *85*, 3533−3539.
(30) Albright, T. A.; Hofmann, P.; Hoffmann, R. *J. Am. Chem. Soc.* **1977**, *99*, 7546−7557.
(31) Lauher, J. W.; Hoffmann, R. *J. Am. Chem. Soc.* **1976**, *98*, 1729−1742.
(32) Elian, M.; Hoffmann, R. *Inorg. Chem.* **1975**, *14*, 1058.
(33) Rossi, A. R.; Hoffmann, R. *Inorg. Chem.* **1975**, *14*, 365−374.
(34) Schilling, B. E.; Hoffmann, R.; Lichtenberger, D. L. *J. Am. Chem. Soc.* **1979**, *101*, 585−591.
(35) Vining, W. J.; Neyhart, G. A.; Nielsen, S.; Sullivan, B. P. *Inorg. Chem.* **1993**, *32*, 4214−4217.
(36) Manna, J.; Kuk, R. J.; Dallinger, R. F.; Hopkins, M. D. *J. Am. Chem. Soc.* **1994**, *116*, 9793−9794.
(37) Abbreviations: DCE, 1,2-dichloroethane; DME, 1,2-dimethoxyethane; py, pyridine; $^t$A, tert-amyl; Ada, 1-adamantyl; $^t$Oct, $CMe_2CH_2CMe_3$; Ar, 2,6-$^i$Pr$_2$-C$_6$H$_3$; Ar′, 2,6-Me$_2$-C$_6$H$_3$; PhCN, 4-CN-C$_6$H$_4$; Nap, 2-naphthyl; Anth, 2-anthryl.
(38) Chao, Y.-W.; Wexler, P. A.; Wigley, D. E. *Inorg. Chem.* **1989**, *28*, 3860−3868.
(39) Clegg, W.; Errington, R. J.; Hockless, D. C. R.; Redshaw, C. *Polyhedron* **1991**, *10*, 1959−1961.
(40) Jayaratne, K. C.; Yap, G. P.; Haggerty, B. S.; Rheingold, A. L.; Winter, C. H. *Inorg. Chem.* **1996**, *35*, 4910−4920.
(41) Churchill, M. R.; Wasserman, H. J. *Inorg. Chem.* **1982**, *21*, 223.
(42) Worl, L. A.; Duesing, R.; Chen, P.; Ciana, L. D.; Meyer, T. J. *J. Chem. Soc., Dalton Trans.* **1991**, 849.

**Table 1.** Absorption and Emission Spectral Data in Optically Dilute ($A < 0.5$) DCE Solutions[37]

| compound | | $^3$(nb,$\pi$) (nm) | $^3$(nb,$\pi$) ($cm^{-1}$) | $\epsilon$ ($M^{-1}$ $cm^{-1}$) | $E_{00}$ ($cm^{-1}$) | $E_{em}$ ($cm^{-1}$) |
|---|---|---|---|---|---|---|
| **1a** | $Ta(NCMe_2Et)Cl_3py_2$ | 373 | 26 800 | 140 | 21 500 | 17 400 |
| **1b** | $[Ta(NCMe_2Et)Cl_5]^{2-}$ | 373 | 26 800 | 85 | 21 700 | 17 900 |
| **1c** | $Ta(NCMe_2Et)Cl_3$(dme) | 343 | 29 200 | 160 | 22 900 | 18 500 |
| **2a** | $Ta(NCMe_3)Cl_3py_2$ | 367 | 27 200 | 140 | 21 600 | 17 400 |
| **2b** | $[Ta(NCMe_3)Cl_5]^{2-}$ | 350 | 28 600 | | 21 700 | 17 700 |
| **2c** | $Ta(NCMe_3)Cl_3$(dme) | 338 | 29 600 | 150 | 22 900 | 18 500 |
| **3a** | $Ta(NCH(CHMe_2)_2)Cl_3py_2$ | 373 | 26 800 | 73 | 21 500 | 17 500 |
| **3b** | $[Ta(NCH(CHMe_2)_2)Cl_5]^{2-}$ | 376 | 26 600 | 120 | 21 800 | 18 000 |
| **3c** | $Ta(NCH(CHMe_2)_2)Cl_3$(dme) | 348 | 28 700 | 100 | 23 200 | 18 900 |
| **4a** | $Ta(NAda)Cl_3py_2$ | 379 | 26 400 | 180 | 21 000 | 17 200 |
| **4c** | $Ta(NAda)Cl_3$(dme) | 352 | 28 400 | 120 | 22 800 | 18 700 |
| **5a** | $Ta(N^tOct)Cl_3py_2$ | 374 | 26 700 | 98 | 21 400 | 17 500 |
| **5b** | $[Ta(N^tOct)Cl_5]^{2-}$ | 370 | 27 000 | 83 | 21 500 | 17 500 |
| **5c** | $Ta(N^tOct)Cl_3$(dme) | 344 | 29 100 | 130 | 22 900 | 18 700 |
| **6a** | $Ta(N^nBu)Cl_3(py)_2$ | 367 | 27 200 | 90 | 21 200 | 17 200 |
| **6b** | $[Ta(N^nBu)Cl_5]^{2-}$ | 351[a] | 28 500[a] | | 21 800 | 17 400 |
| **6c** | $Ta(N^nBu)Cl_3$(dme) | 342 | 29 200 | 130 | 23 100 | 18 500 |
| **7** | $Ta(NPh)Cl_3$(dme) | 425 | 23 500 | 110 | 19 200 | 15 900 |
| **8a** | $Ta(NAr)Cl_3py_2$ | 478 | 20 900 | 99 | | 14 600 |
| **8c** | $Ta(NAr)Cl_3$(dme) | 445 | 22 500 | 130 | 18 100 | 15 000 |
| **9** | $Ta(NAr')Cl_3$(dme) | 443 | 22 600 | 150 | 18 100 | 15 000 |
| **10** | $Ta(NPhCN)Cl_3$(dme) | 400 (sh) | 25 000 | 220 | 20 200 | 17 000 |
| **11** | $Ta(NNap)Cl_3$(dme) | 438 | 22 800 | 200 | 18 300 | 15 200 |
| **12** | $Ta(NAnth)Cl_3$(dme) | 460 (sh) | 21 700 | 500 | | – |
| **13b** | $[Nb(NCMe_2Et)Cl_5]^{2-}$ | 402 | 24 900 | 35 | 19 400 | 15 200 |
| **13c** | $Nb(NCMe_2Et)Cl_3$(dme) | 377 | 26 500 | 71 | 20 000 | 15 400 |
| **14** | $Nb(NCMe_3)Cl_3$(dme) | 378 | 26 500 | 69 | 20 100 | 15 400 |
| **15** | $Nb(NAda)Cl_3$(dme) | 387 | 25 800 | 77 | 20 000 | 15 400 |
| **16** | $Nb(NPh)Cl_3$(dme) | 484 | 20 700 | 39 | 16 100 | 13 300 |
| **17** | $Nb(NPhCN)Cl_3$(dme) | 460 | 21 800 | 44 | 17 300 | 14 100 |

phen)$Re(CO)_3Cl$ ($\lambda_{max} = 36\,800$ $cm^{-1}$), a difference of ~1200 $cm^{-1}$ between H and Ph.[43]

The UV transitions are much more intense ($6000 < \epsilon < 15\,000$ $M^{-1}$ $cm^{-1}$) than those in the visible region (Figure 1). Again there is a significant difference between aryl and alkyl imido spectral profiles. In the aryl imidos, Band II appears in the region of the lowest-energy transition of the free amine (~34 000 $cm^{-1}$; **8c**) but at higher energy (~38 000 $cm^{-1}$) in the alkyl imidos. Figure 1b compares absorption spectra of aniline and $Ta(NPh)Cl_3$(dme) (**7**). The free amine transition ($L_b$)[44] occurs at approximately the same energy as Band II in **7** but is sharper and much less intense. Structured absorption spectra are noted in the 2-naphthyl and 2-anthryl imido compounds and resemble those of the amines.[44] A more detailed investigation of Band II in the aryl imidos will be the subject of a future report.

Band III (~42 500 $cm^{-1}$; **1c**) occurs near the solvent limit in each case, at similar energy to the Ta ← Cl charge-transfer transitions in $TaCl_5L$ (L = Lewis base, halide).[45,46] Band III is observed at lower intensity and occurs at somewhat higher energy than the LMCT absorptions in the complex halides. For comparison, spectra of $TaCl_5(OEt_2)$ in DCE, **1c**, and **7** are plotted together in Figure 1c. Previously reported data were acquired in MeCN[45] but are similar to those we recorded using DCE solvent. Absorption profiles of $TaCl_5(OR_2)$ and $[TaCl_6]^-$ [46] are not substantially different. The observed structured absorption bands in $[TaCl_6]^-$ are assigned as LMCT ($2t_{2g}$ (Ta) ← (Cl) $1t_{1u}$, $2t_{1u}$, and $1t_{2u}$).[46]

**Solution Luminescence.** All of the compounds reported here exhibit green to orange emission in both the solid state and solution at room temperature upon excitation into the lowest-energy absorption band. There is a substantial dependence of emission energy on the imido substituent, similar to that observed in the absorption spectra. Representative emission profiles for $Ta(NR)Cl_3$(dme) (R = $CH^iPr_2$ (**3c**), 2,6-$^iPr_2C_6H_3$ (**8c**)) are shown in Figure 2 with the corresponding absorption or excitation spectra at higher energy. The emission bands were corrected for spectrometer response and are broad and featureless both at room temperature and at 77 K ($\Delta\bar{\nu}_{1/2} \sim 5000$ $cm^{-1}$). Emission profiles and maxima are concentration and excitation wavelength independent throughout the region of the lowest-energy absorption. Stokes' shifts are quite large, ranging from ~7500 $cm^{-1}$ in compounds **8** to nearly 11 000 $cm^{-1}$ in compounds **2**. This combined with the symmetric shape of the emission (and excitation) profiles is consistent with a large excited-state distortion. The exception here is the anthrylimido compound (**12**), in which there is no measurable emission in our hands, likely due to low emission energy and quantum yield expected for this compound (vide infra). Emission spectra for the niobium compounds do not differ significantly from their tantalum congeners with the exception that the emission maxima occur at lower energies, as observed in the absorption spectra.

Excitation spectra overlay the low-energy absorption profiles, with some discrepancies at the high-energy side of the band due to overlap of the lowest-energy absorption with the tail of intense higher-energy absorptions. There is some wavelength dependence on emission quantum yield in the arene region of the aryl imido compounds—excitation in this region does not populate the emissive excited state with unit efficiency.

**Comparison of Absorption/Emission Spectra.** Because the low-energy tail of the absorption spectra overlap the high-energy tail of emission spectra, we sought to determine $E_{00}$, the energy

(43) Wrighton, M.; Morse, D. L. *J. Am. Chem. Soc.* **1974**, *96*, 998−1003.
(44) Döller, E.; Förster, T.; Renner, H. *Z. Phys. Chem. Neue Folge* **1958**, *15*, 34−47.
(45) Valloton, M.; Merbach, A. E. *Helv. Chim. Acta* **1975**, *58*, 2272−2283.
(46) Valloton, M.; Merbach, A. E. *Helv. Chim. Acta* **1974**, *57*, 2345−2356.

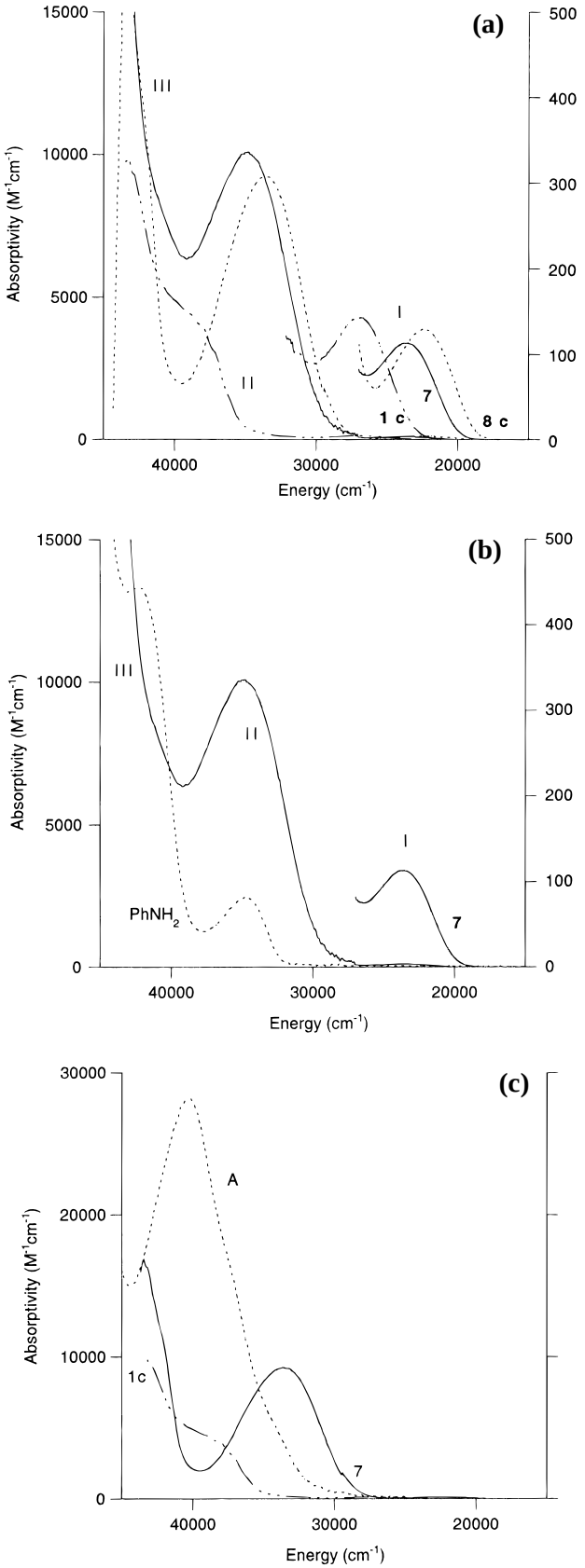


**Figure 1.** (a) Absorption spectra of $Ta(NCMe_2Et)Cl_3(dme)$ (**1c**; · · · — · · ·), $Ta(NPh)Cl_3(dme)$ (**7**; —), and $Ta(NAr)Cl_3(dme)$ (**8c**; - - -) at 295 K in DCE solutions. The low-energy region on the right is plotted on an expanded axis. (b) Absorption spectra of $Ta(NPh)Cl_3(dme)$ (**7**; —) and aniline (- - -) at 295 K in DCE solution. (c) UV absorption profiles of $Ta(NCMe_2Et)Cl_3(dme)$ (**1c**; · · · — · · ·), $Ta(NPh)Cl_3(dme)$ (**7**; —) $TaCl_5(OEt_2)$ (**A**; - - -) at 295 K in DCE solutions.

of the electronic transition between the lowest-energy vibrational states, $v_0^* \rightarrow v_0$, by quantitative comparison of the spectra. The spectra were corrected for nonlinear grating response (with $\bar{\nu}$) and were plotted as follows: The absorption or excitation data were plotted as intensity over energy vs energy, $(I(\bar{\nu})/\bar{\nu})$ vs $\bar{\nu}$, and emission spectra were converted into intensity over energy cubed vs energy, $(I(\bar{\nu})/\bar{\nu}^3)$ vs $\bar{\nu}$, according to the method of Birks and Dyson.[47] The spectral maxima were both normalized to a scale of 1000, rather than using the reported method.[47] The overlap and near mirror image relationship of emission spectra with absorption or excitation spectra are consistent with absorption into and emission from the same state.[47] Calculated values for $E_{00}$ determined by this method are included in Table 1. Absorption band profiles are slightly distorted compared to the excitation spectra in some cases, but this appears to be a negligible complication; values determined from either absorption or excitation spectra agree within ~200 $cm^{-1}$, Figure 2. The absorption and emission mirror profiles are overlaid for the most part, with some discrepancy in the low-energy region of **8c**.

**Excited-State Deactivation: Emission Lifetimes and Quantum Yields.** Rates of excited-state decay ($k_{obs}$ or $1/\tau$) were determined using either of two techniques. For short-lived emitters, a Spex Fluorolog $\tau 2$ phase-shift fluorimeter was used ($\tau < 1$ $\mu$s). For longer-lived samples, a standard laser flash photolysis experiment was used. Excitation into the low-energy tail of the absorption band was used as a rule, however, $k_{obs}$ was independent both of excitation wavelength (throughout Band I) and monitoring wavelength in each case. Single-exponential fits satisfactorily describe the observed decay of emission intensity with time. When convenient (chromophores with lifetimes in the range $50 < \tau < 1000$ ns), both instruments were used and good agreement between them was obtained. Emission lifetimes in solution at room temperature ranged from 50 ns (**8a**) to 17 $\mu$s (**1c**), approximately 2 orders of magnitude over a range of ~4500 $cm^{-1}$ in emission energies. Compounds with the highest emission energies in this series also had (roughly) the longest observed excited-state lifetimes (or smallest $k_{obs}$). The data are presented in Table 2.

Quantum yields for these compounds were determined by comparison of integrated emission spectra with those of aerated $[Ru(bpy)_3]^{2+}$ in acetonitrile ($\phi_{em} = 0.012$) or quinine sulfate in 1 N $H_2SO_4$ ($\phi_{em} = 0.51$) as emission standards, according to Demas and Crosby.[48] The quantum yields of both standards are invariant with excitation wavelength over broad range. Where convenient, both standards were used to check for consistency. In general, emission quantum yields are large and variable in these compounds, ranging from less than 0.001 to as high as 0.24, Table 2. Alkyl imido compounds have the largest emission energies and quantum yields, up to 23 000 $cm^{-1}$ and 0.24, respectively. The cyanophenyl and phenyl imidos have somewhat lower quantum yields, and substituted aryl imidos have the lowest. There is a much smaller effect on $\phi_{em}$ observed when changing the Lewis base ligands, with the dme adducts having the larger quantum yields than, e.g., the pyridine adducts in each series. The imido substituent is the major factor affecting quantum yield. The niobium compounds generally exhibited lower emission quantum yields and lifetimes.

Rates for the radiative ($k_r$) and nonradiative ($k_{nr}$) excited-state decay processes are readily obtained from these data; $k_r = \phi_{em}/\tau$ and $k_{nr} = (1 - \phi_{em})/\tau$.[48] As might be expected, radiative deactivation rates for the niobium compounds are

(47) Birks, J. B.; Dyson, D. J. *Proc. R. Soc.* **1963**, *275 A*, 135−148.
(48) Demas, J. N.; Crosby, G. A. *J. Phys. Chem.* **1971**, *75*, 991−1024.

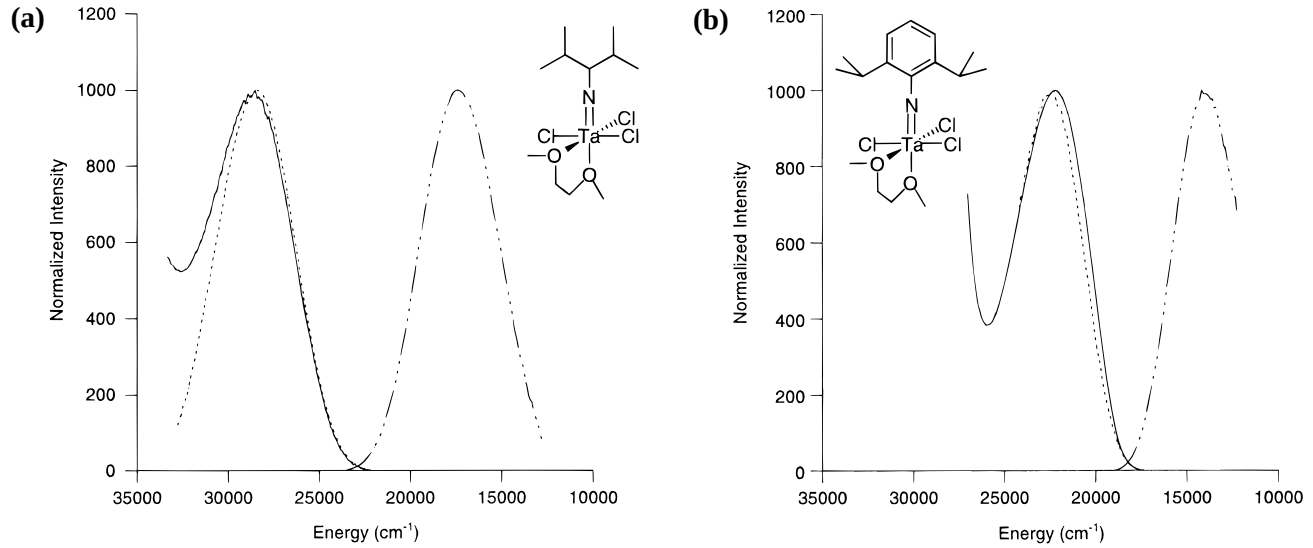


**Figure 2.** (a) Plots of absorption ($\epsilon(\bar{\nu})/\bar{\nu}$ vs $\bar{\nu}$; —), emission ($F(\bar{\nu})/\bar{\nu}^3$ vs $\bar{\nu}$; · · · — · · ·), and the mirror image of emission ($F(2\bar{\nu}_0 - \bar{\nu})/(2\bar{\nu}_0 - \bar{\nu})^3$ vs $\bar{\nu}$; - - -) spectra of Ta(NCMe$_2$Et)Cl$_3$(dme) (**1c**) at 295 K in DCE solution. (b) Plots of absorption ($\epsilon(\bar{\nu})/\bar{\nu}$ vs $\bar{\nu}$; —), emission ($F(\bar{\nu})/\bar{\nu}^3$ vs $\bar{\nu}$; · · · — · · ·), and the mirror image of emission ($F(2\bar{\nu}_0 - \bar{\nu})/(2\bar{\nu}_0 - \bar{\nu})^3$ vs $\bar{\nu}$; - - -) spectra of Ta(NAr)Cl$_3$(dme) (**8c**) at 295 K in DCE solution.

**Table 2.** Excited State Data for Tantalum Imido Compounds in 1,2-DCE[44]

| | compound | $\phi_{em}$ | $\tau$ (ns) | $k_{nr}$ ($10^4$ s$^{-1}$) | $k_r$ ($10^4$ s$^{-1}$) | $k_r$(calcd) ($10^4$ s$^{-1}$) |
|---|---|---|---|---|---|---|
| **1a** | Ta(NCMe$_2$Et)Cl$_3$py$_2$ | 0.10 | 9 100 | 9.9 | 1.1 | 54 |
| **1b** | [Ta(NCMe$_2$Et)Cl$_5$]$^{2-}$ | 0.11 | 10 000 | 8.9 | 1.1 | 34 |
| **1c** | Ta(NCMe$_2$Et)Cl$_3$(dme) | 0.24 | 17 000 | 4.5 | 1.4 | 68 |
| **2a** | Ta(NCMe$_3$)Cl$_3$py$_2$ | 0.09 | 9 400 | 9.7 | 1.0 | 53 |
| **2b** | [Ta(NCMe$_3$)Cl$_5$]$^{2-}$ | 0.06 | 10 500 | 9.0 | 0.6 | – |
| **2c** | Ta(NCMe$_3$)Cl$_3$(dme) | 0.19 | 17 200 | 4.7 | 1.1 | 65 |
| **3a** | Ta(NCH(CHMe$_2$)$_2$)Cl$_3$py$_2$ | 0.08 | 5 500 | 17 | 1.5 | 28 |
| **3b** | [Ta(NCH(CHMe$_2$)$_2$)Cl$_5$]$^{2-}$ | 0.11 | 7 500 | 12 | 1.5 | 50 |
| **3c** | Ta(NCH(CHMe$_2$)$_2$)Cl$_3$(dme) | 0.20 | 11 900 | 7 | 1.7 | 44 |
| **4a** | Ta(NAda)Cl$_3$py$_2$ | 0.10 | 6 000 | 15 | 1.6 | 66 |
| **4c** | Ta(NAda)Cl$_3$(dme) | 0.20 | 15 000 | 5 | 1.3 | 50 |
| **5a** | Ta(N$^t$Oct)Cl$_3$py$_2$ | 0.06 | 4 200 | 22 | 1.5 | 38 |
| **5b** | [Ta(N$^t$Oct)Cl$_5$]$^{2-}$ | 0.027 | 3 700 | 26 | 0.7 | 33 |
| **5c** | Ta(N$^t$Oct)Cl$_3$(dme) | 0.04 | 2 300 | 42 | 1.9 | 59 |
| **6a** | Ta(N$^n$Bu)Cl$_3$(py)$_2$ | 0.023 | 3 700 | 26 | 0.6 | – |
| **6b** | [Ta(N$^n$Bu)Cl$_5$]$^{2-}$ | 0.03 | 5 100 | 19 | 0.6 | 32 |
| **6c** | Ta(N$^n$Bu)Cl$_3$(dme) | 0.13 | 8 700 | 10 | 1.5 | 56 |
| **7** | Ta(NPh)Cl$_3$(dme) | 0.008 | 200 | 500 | 4.1 | 36 |
| **8a** | Ta(NAr)Cl$_3$py$_2$ | 0.0008 | 50 | 2000 | 1.6 | 26 |
| **8c** | Ta(NAr)Cl$_3$(dme) | 0.0015 | 65 | 1500 | 2.3 | 37 |
| **9** | Ta(NAr′)Cl$_3$(dme) | 0.0022 | 72 | 1400 | 3.1 | 46 |
| **10** | Ta(NPhCN)Cl$_3$(dme) | 0.017 | 2 100 | 47 | 0.8 | – |
| **11** | Ta(NNap)Cl$_3$(dme) | 0.0021 | 81 | 1200 | 2.6 | 59 |
| **12** | Ta(NAnth)Cl$_3$(dme) | – | – | – | – | – |
| **13b** | [Nb(NCMe$_2$Et)Cl$_5$]$^{2-}$ | 0.005 | 1 900 | 51 | 0.26 | |
| **13c** | Nb(NCMe$_2$Et)Cl$_3$(dme) | 0.008 | 2 300 | 43 | 0.36 | |
| **14** | Nb(NCMe$_3$)Cl$_3$(dme) | 0.007 | 2 000 | 50 | 0.35 | |
| **15** | Nb(NAda)Cl$_3$(dme) | 0.0078 | 3 000 | 33 | 0.26 | |
| **16** | Nb(NPh)Cl$_3$(dme) | 0.00012 | 30 | 3300 | 0.4 | |
| **17** | Nb(PhCN)Cl$_3$(dme) | 0.0006 | 110 | 910 | 0.55 | |

approximately an order of magnitude smaller than observed for the tantalum compounds. Under the experimental conditions reported here, each chromophore is photostable, except **11** and **12**. Data for these two compounds were acquired immediately after sample preparation in the dark, and only slight variation in the sample absorption spectrum was noted throughout the data acquisition time frame.

**Excited-State Quenching.** The luminescence observed from these compounds in solution is readily quenched by anthracene, amines, and other commonly used electron- and energy-transfer quenching reagents. For example, anthracene quenching obeys classic Stern−Volmer kinetics in emission quenching of **10** with a rate constant $k_q = 4.5 \times 10^9$ M$^{-1}$ s$^{-1}$ in a pseudo-first-order reaction. This is consistent with the excited state being primarily triplet in character.[49] A full report of these phenomena will be published at a later date.

**Electrochemistry.** Electrochemistry was carried out in DCE using 0.1 M [$^n$Bu$_4$N][PF$_6$] as electrolyte, referenced to Cp$_2$Fe$^{+/0}$ (internal). Both oxidative and reductive processes were irreversible even at high scan rates, and little useful information was obtained.

## PM3 Calculations

To investigate the origin of the dramatic aryl effect on the absorption spectra of these imido compounds, we calculated

(49) Calvert, J. G.; Pitts, J. N. *Photochemistry*; Wiley: New York, 1966.

**Table 3.** Pertinent Bond Lengths and Angles for $[Ta(NPh)Cl_5]^-$ and $[Ta(N^tBu)Cl_5]^-$ Models Used in the Calculations[a]

| | bond | length (Å) | bonds | angle (deg) |
|---|---|---|---|---|
| $[Ta(N^tBu)Cl_5]^-$ | Ta═N | 1.731 | Ta−N−C | 179.5 |
| | Ta−Cl (*cis*) | 2.44 | N−Ta−Cl (*cis*) | 97.5 |
| | Ta−Cl (*trans*) | 2.695 | N−Ta−Cl (*trans*) | 180 |
| | N−C | 1.454 | | |
| $[Ta(NPh)Cl_5]^-$ | Ta═N | 1.773 | Ta−N−C | 180 |
| | Ta−Cl (*cis*) | 2.42 | N−Ta−Cl (*cis*) | 97.5 |
| | Ta−Cl (*trans*) | 2.695 | N−Ta−Cl (*trans*) | 180 |
| | N−C | 1.38 | | |
| $[Nb(NCMe_3)Cl_4(py)]^-$ | Nb═N | 1.731 | Nb−N−C | 176.4(4) |
| | Nb−Cl (*cis*) | ∼2.44 | N−Nb−Cl (*cis*) | ∼97 |
| | Nb-py (*trans*) | 2.479(4) | N−Nb-py (*trans*) | 177.8(2) |
| $[Ta(NAr)Cl_5]^{2-}$ | Ta═N | 1.773(8) | Ta−N−C | 176.2(7) |
| | Ta−Cl (*cis*) | ∼2.42 | N−Ta−Cl (*cis*) | ∼97.5 |
| | Ta−Cl (*trans*) | 2.695(3) | N−Ta−Cl (*trans*) | 175.5(2) |

[a] Lengths and angles for $[Nb(NCMe_3)Cl_4(py)]^-$ and $[Ta(NAr)Cl_5]^{2-}$ are experimental values included for comparison, taken from refs 39 and 40.

**Chart 1.** Structures of $[Ta(NCMe_3)Cl_5]^{2-}$ and $[Ta(NPh)Cl_5]^{2-}$ Used for the Calculations

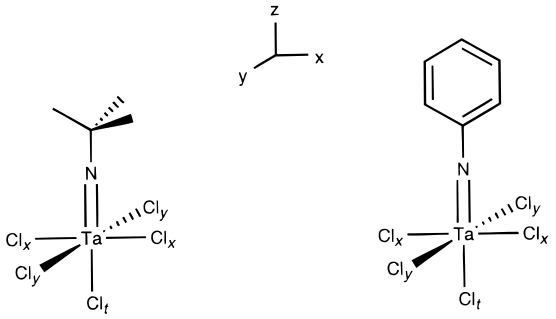


the electronic structures of $[Ta(NCMe_3)Cl_5]^{2-}$ and $[Ta(NPh)Cl_5]^{2-}$ using MacSpartan Plus[50] and the PM3 method.[51] Models were constructed using averaged experimental data[39,40] from axially symmetric octahedra, and the metrical parameters are listed in Table 3. The trans chloride in $[Ta(NAr)Cl_5]^{2-}$ is hydrogen bonded to two pyridinium cations in the solid-state structure, resulting in a 2.695 Å bond length,[40] comparable to that observed in the chloride-bridged $[Ta(N^tBu)(NH^tBu)(NH_2tBu)\text{-}Cl]_2(\mu\text{-}Cl)_2$, 2.687 Å (a low-quality structure).[52] Other crystallographically characterized group 5 imidos with a trans chloride involve bridging chloride ligands, with trans RN−Ta−Cl bond lengths of ∼2.8 Å. Examples of group 6 compounds, such as mer-$W(NAr)Cl_3(PMe_3)_2$, have significantly shorter trans chloride distances, in this case 2.49 Å. We therefore used a *trans*-Cl distance of 2.695 Å, which is probably too long. Averaged values for the equatorial chlorides were used in order to provide molecules with $C_{4v}$ local symmetry at the metal center, improving the clarity of the results.

Since orbital energies calculated by these methods are likely to be poor estimates, we avoid a discussion of them. We discuss the $\pi$-bonding structure of the *tert*-butyl alkyl in some detail and point to the differences observed with the phenyl compound. For reference, Chart 1 shows the minimized geometries used in the MO calculation, with coordinate axes. As shown, the *xz* plane is coincident with the plane of the page, and the alkyl substituents are oriented exactly as drawn.

In Table 4, pertinent orbitals in $[Ta(N^tBu)Cl_5]^{2-}$ are listed with their percentage atomic and orbital characters. The lowest-energy orbitals with significant Ta−N $\pi$ character are the degenerate HOMO(−14) and HOMO(−13), which are Ta═N $\pi$-bonding, and include significant $\pi$-bonding interactions from the equatorial chlorides. These orbitals are almost 1/3 each metal d and equatorial chloride p in character, highly delocalized over the entire molecule, including 10% on the alkyl substituent. Very close in energy is HOMO(−12), which is $d_{xy}$−Cl p $\pi$-bonding, again a delocalized orbital which is 16% metal d. Another degenerate pair of Ta═N $\pi$-bonding orbitals exists in HOMO(−4), HOMO(−3), which are now Ta−$Cl_{eq}$ $\pi$* in

**Table 4.** Percentage Orbital Contributions in Pertinent Orbitals of $[Ta(N^tBu)Cl_5]^-$

| orbital | energy (eV) | percentage | atom | orbital character (%) |
|---|---|---|---|---|
| HOMO(-14) | −5.356 | 27.6 | Ta | $d_{xz}$ (54), $d_{yz}$ (46) |
| $\pi$ | | 25.3 | N | $p_x$ (54), $p_y$ (46) |
| | | 10.7 | alkyl | |
| | | 9.8 | $Cl_x$ (2) | $p_z$ (84) |
| | | 6.6 | $Cl_y$(2) | $p_z$ (82) |
| | | 3.3 | $Cl_t$ | $P_x$ (55), $p_y$ (45) |
| HOMO(-13) | −5.355 | 27.6 | Ta | $d_{yz}$ (54), $d_{xz}$ (46) |
| $\pi$ | | 25.3 | N | $p_y$ (54), $p_x$ (46) |
| | | 10.6 | alkyl | |
| | | 6.6 | $Cl_x$ (2) | $p_z$ (82) |
| | | 10.0 | $Cl_y$ (2) | $p_z$ (83) |
| | | 3.3 | $Cl_t$ | $p_y$ (55), $p_x$ (45) |
| HOMO(-12) | −4.747 | 15.9 | Ta | $d_{xy}$ (99) |
| $nb_B$ | | 21 | $Cl_x$ (2) | $p_y$ (100) |
| | | 21 | $Cl_y$ (2) | $p_x$ (100) |
| HOMO(-4) | −2.454 | 3.8 | Ta | $d_{xz}$ (71), $d_{yz}$ (26) |
| $\pi$ | | 29.5 | N | $p_x$ (73), $p_y$ (27) |
| | | 2.9 | alkyl | |
| | | 21.1 | $Cl_x$ (2) | $p_z$ (89) |
| | | 10.7 | $Cl_y$ (2) | $p_z$ (80) |
| | | 0.5 | $Cl_t$ | $p_x$ (80) |
| HOMO(-3) | −2.453 | 3.8 | Ta | $d_{yz}$ (71), $d_{xz}$ (26) |
| $\pi$ | | 29.5 | N | $p_y$ (73), $p_x$ (27) |
| | | 2.9 | alkyl | |
| | | 10.7 | $Cl_x$ (2) | $p_z$ (86) |
| | | 21.1 | $Cl_y$ (2) | $p_z$ (88) |
| | | 0.5 | $Cl_t$ | $p_y$ (80) |
| LUMO(+1) | 8.584 | 83.8 | Ta | $d_{xy}$ (100) |
| $nb_A$ | | 4 | $Cl_x$ (2) | $p_y$ (100) |
| | | 4 | $Cl_y$ (2) | $p_x$ (100) |
| LUMO(+12) | 10.027 | 37.5 | Ta | $d_{yz}$ (98) |
| $\pi$* | | 14.7 | N | $p_y$ (98) |
| | | 44.4 | alkyl | |
| LUMO(+13) | 10.029 | 37.6 | Ta | $d_{yz}$ (98) |
| $\pi$* | | 14.8 | N | $p_y$ (98) |
| | | 43.9 | alkyl | |

(50) Wave function, I. *MacSpartan Plus*, Release 1.0.4; Wavefunction, Inc.: 18401 Von Karman Ave., No. 370, Irvine, CA 92715, 1996.
(51) Stewart, J. J. R. *J. Computer Aided Molecular Design* **1990**, *4*, 1.
(52) Jones, T. C.; Nielson, A. J.; Rickard, C. E. F. *Chem. Commun.* **1984**, 205−206.

**Chart 2.** Pictorial Representation of Pertinent $\pi$-Orbital Interactions for $[Ta(NCMe_3)Cl_5]^{2-}$ Based on the MacSpartan Calculation

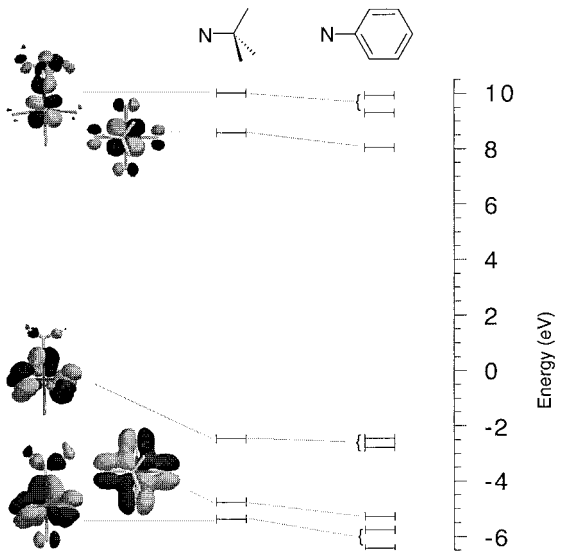


character and are highly N-localized ($\sim$ 30%). These orbitals have little tantalum character (4%). The calculated HOMO, HOMO($-1$), and HOMO($-2$) are ligand-centered nonbonding orbitals involving the chlorides. LUMO($+1$) is primarily $d_{xy}$ (84%) and the antibonding component of HOMO($-12$). Finally, LUMO($+12$) and LUMO($+13$) represent the Ta=N $\pi^*$ orbitals, which are again a degenerate pair. They are primarily localized on Ta (38%) and the alkyl substituent (44%). Chart 2 provides a simplified pictorial representation of the energy levels in the calculated structures.

The results for the phenylimido compound are somewhat more complicated; however, the primary difference is a splitting of the three degenerate pairs of Ta=N $\pi$-type orbitals (Chart 2) and a dramatic increase in the alkyl character of the Ta=N $\pi$ interaction perpendicular to the arene, as listed in Table 5. The magnitude of this splitting is between 0.3 and 0.7 eV. One can see the significant arene character in the $\pi$ system perpendicular to the ring (labeled $\pi_\perp$).

The Ta$-$N $\pi$-bonding orbitals (approximate HOMOs) are shown pictorially in Figure 3. There is a clear aryl effect: significant interaction of the aryl $\pi$ system with the Ta$-$N $\pi$ system is evident perpendicular to the aryl plane. This suggests a significant electronic change in the aryl imidos which is manifested in the lowest-excited state energy, lifetime, and quantum yields in these compounds. From these results one can see that even a simplified treatment of the bonding in these compounds differs significantly from the highly useful "back-of-the-envelope" type MO calculation shown in Chart 3, commonly used by synthetic chemists to think about bonding and reactivity.

## Discussion

**Spectral Assignments.** If we consider the electronic structure of these compounds based on that of $TaCl_5L$ (L = Lewis base, $Cl^-$),[45,46] a clear bonding picture emerges. In $[TaCl_6]^-$, the splitting of $t_{2g}$ and $e_g$ is small,[46] as is the splitting of $t_{2g}$ upon substituting $Me_2O$ for a chloride in $C_{4v}$ $TaCl_5L$.[45] Intense UV transitions in these species are assigned as Ta $\leftarrow$ Cl charge transfer (LMCT), specifically $^1(2t_{2g} \leftarrow 1t_{1g}, 2t_{1u}, 1t_{2u}$, and $1t_{1u})$ in the hexachlorometalates(V). The UV spectrum of $TaCl_5(OEt_2)$ is shown in Figure 1c, with **1c** and **7** for comparison.

**Table 5.** Percentage Orbital Contributions in Pertinent Orbitals of $[Ta(NPh)Cl_5]^-$

| orbital | energy (eV) | percentage | atom | orbital character (%) |
|---|---|---|---|---|
| HOMO(-17) | $-6.427$ | 19.1 | Ta | $d_{yz}$ (100) |
| $\Pi_\perp$ | | 28.6 | N | $p_y$ (100) |
| | | 36.3 | alkyl | |
| | | – | $Cl_x$ (2) | |
| | | 7.1 | $Cl_y$ (2) | $p_z$ (86) |
| | | 1.4 | $Cl_t$ | $p_y$ (100) |
| HOMO(-15) | $-5.76$ | 27.8 | Ta | $d_{xz}$ (100) |
| $\pi_{//}$ | | 24.2 | N | $p_x$ (100) |
| | | 9.7 | alkyl | |
| | | 17.3 | $Cl_x$ (2) | $p_z$ (82) |
| | | 0.2 | $Cl_y$ (2) | |
| | | 3.4 | $Cl_t$ | $p_x$ (100) |
| HOMO(-14) | $-5.274$ | 17.7 | Ta | $d_{xy}$ (100) |
| $nb_B$ | | 20.9 | $Cl_x$ (2) | $p_y$ (100) |
| | | 20.9 | $Cl_y$ (2) | $p_x$ (100) |
| HOMO(-4) | $-2.78$ | 3.6 | Ta | $d_{xz}$ (89) |
| $\pi_{//}$ | | 32.4 | N | $p_x$ (100) |
| | | 3.1 | alkyl | |
| | | 29.3 | $Cl_x$ (2) | $p_z$ (88) |
| | | 1 | $Cl_y$ (2) | |
| | | 0.3 | $Cl_t$ | |
| HOMO(-2) | $-2.448$ | 3.8 | Ta | $d_{yz}$ (97) |
| $\pi_\perp$ | | 21.9 | N | $p_y$ (100) |
| | | 24.7 | alkyl | |
| | | 0.1 | $Cl_x$ (2) | |
| | | 18.7 | $Cl_y$ (2) | $p_z$ (80) |
| | | 11.7 | $Cl_t$ | $p_y$ (100) |
| LUMO(+4) | 8.041 | 82.3 | Ta | $d_{xy}$ (100) |
| $nb_M$ | | 4.4 | $Cl_x$ (2) | $p_y$ (100) |
| | | 4.4 | $Cl_y$ (2) | $p_x$ (100) |
| LUMO(+10) | 9.298 | 45.7 | Ta | $d_{xz}$ (100) |
| $\pi_{//}^*$ | | 17.3 | N | $p_x$ (100) |
| | | 32.4 | alkyl | |
| | | 2 | $Cl_x$ (2) | $p_z$ (65) |
| | | – | $Cl_y$ (2) | |
| | | 0.7 | $Cl_t$ | |
| LUMO(+12) | 9.929 | 52 | Ta | $d_{yz}$ (100) |
| $\pi_\perp^*$ | | 29.9 | N | $p_y$ (100) |
| | | 13.2 | alkyl | |
| | | – | $Cl_x$ (2) | |
| | | 2 | $Cl_y$ (2) | $p_z$ (65) |
| | | 0.7 | $Cl_t$ | |

The LMCT absorptions in $TaCl_5L$ occur at only slightly lower energy than Band III in the imido compounds, as shown in Figure 1. On the basis of these observations, we assign Band III in Figure 1 to LMCT absorptions (Ta $\leftarrow$ Cl).

By replacing a $Cl^-$ (along $z$) with an imido, forming *trans*-$[Ta(NR)Cl_4L]^-$, we still have a $C_{4v}$ species but the $d_{xy}-(d_{xz}, d_{yz})$ splitting should now be pronounced compared to that in $TaCl_5L$. In Chart 3 a molecular orbital interaction diagram is depicted between the N $p_{x,y}$ and $t_{2g}$ giving the $\pi$, $nb_M$, $\pi^*$ ordering. This simplified picture can be compared with Chart 2 and Figure 3. Replacement of an equatorial $Cl^-$ with an ether should result in a small splitting of the degenerate $(d_{xz}, d_{yz})$[45] which, if significant, is unresolvable due to the broadness of the spectra. This is consistent with the LUMO being primarily nonbonding, for which $d_{xy}$ seems a reasonable assignment, as it should interact only slightly with the weakly $\pi$-donating equatorial ligands. Since $\pi_{MN}$ is filled, the lowest-energy transition should be $nb_M \leftarrow \pi_{MN}$ instead of Ta $\leftarrow$ Cl CT. The universal irreversibility of oxidation processes in these compounds are consistent with the HOMO being the strongly bonding Ta=N $\pi$ interaction.

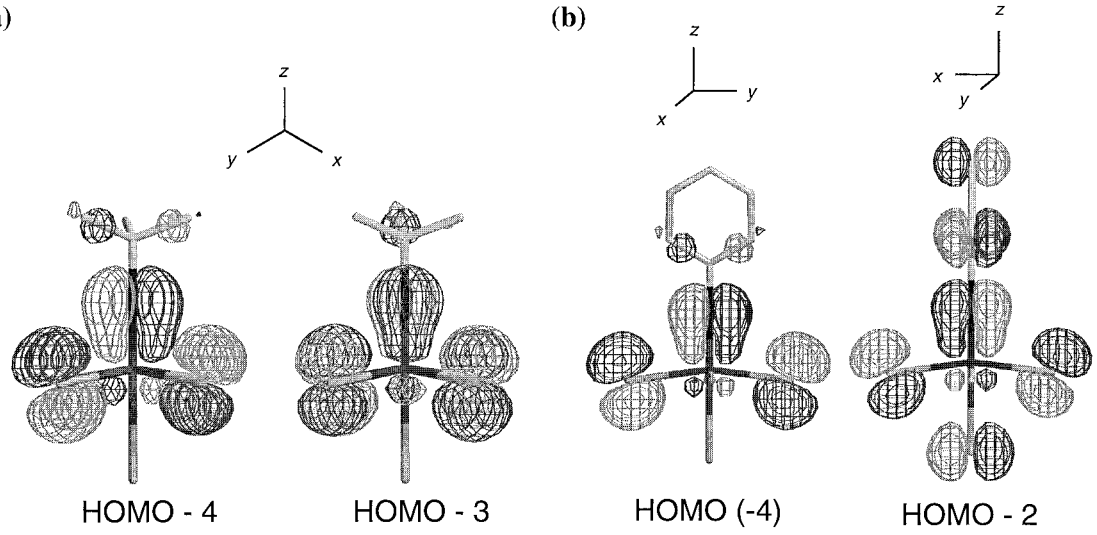


**Figure 3.** (a) Plots of HOMO(−4) and HOMO(−3) of $[Ta(NCMe_3)Cl_5]^{2-}$. (b) Plots of HOMO(−4) and HOMO(−2) of $[Ta(NPh)Cl_5]^{2-}$.

**Chart 3.** Simplified $\pi$-Orbital Interaction Diagram in $d^0$ Imidos with Alkyl and Aryl Substituents

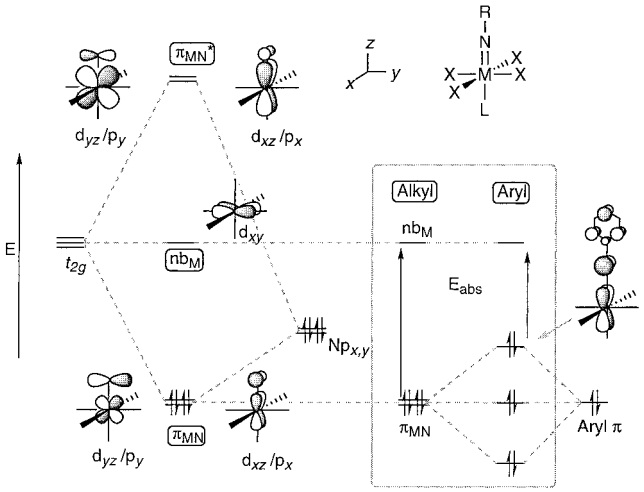


Depending on the magnitude of the N p, M d interactions and the effective dipole length, this $nb_M \leftarrow \pi_{MN}$ transition might be labeled CT, as suggested by the LMCT notation;[16] $L_2Cl_3Ta(NR) \rightarrow L_2Cl_3Ta^-(N^+R)$. The main evidence against a CT assignment is the absence of a solvent dependence on the absorption and emission spectra in these compounds. (This could be due to steric protection from interactions with the solvent by the bulky R groups in these imidos, however.) Additionally, these transitions occur in the same region as and have similar molar absorptivity to the $^2E_g \leftarrow {}^2T_{2g}$ (or $^2(e_g \leftarrow t_{2g})$) transition in $[MCl_6]^{2-}$.[53] The increase in absorptivity and $k_r$ of Band I and its emission partner from Nb to Ta is consistent with a metal centered transition. The distortion observed upon population of the excited state is likely due to depopulation of the $\pi_{MN}$ orbital, which leads to a significant bond length change. Evidence for the metal−imido character of this state is clear based on observation of Band I in all of these compounds. There is no similar absorption band in $[TaCl_6]^-$ or $Ta_2Cl_{10}$.[45,46] Emission from the alkyl imido pentachloride anions $[Ta(NR)Cl_5]^{2-}$ is similarly convincing; no significant emission is observed in the complex halides in solution at room temperature.

Based on overlap of the absorption and emission profiles and their mirror image relationship (Figure 2), it is apparent that the emissive excited state is directly populated upon excitation into Band I. The increase in molar absorptivity upon substituting tantalum for niobium is consistent with a spin-forbidden transition in which the spin selection rule is relaxed by spin−orbit coupling. Since $\epsilon \sim 130$ (Ta) or $\sim 50$ (Nb) and $k_r \sim 10^4$ $s^{-1}$ (Ta) or $\sim 10^3$ $s^{-1}$ (Nb), we assume that absorption into the lowest-energy state and emission from it is formally spin forbidden. We therefore assign the transitions as $^3(nb_M, \pi_{MN}) \leftarrow {}^1A$ (absorption; $C_s$ point group notation) and $^1A \leftarrow {}^3(nb_M, \pi_{MN})$ (emission), with the obvious caveat that the spin character of these transitions is ambiguous due to significant spin−orbit coupling.

At higher energies in the aryl compounds, there is significant absorption in the region of arene absorption, Band II. This band is much more broad and intense than the absorption observed in the amines at similar energy (Figure 1b) and presumably includes the arene $L_b$ absorption. Band II is observed in the alkyl imido compounds at somewhat higher energies, appearing as a less intense shoulder on Band III. With these observations in mind, we tentatively assign Band II in the alkyl imidos as $^1(nb_M, \pi_{MN})$. In the more complex aryl imido spectra, the presence of this transition, $^1L_b$, and transitions from $\pi_{MN}$ to the arene $\pi^*$ system (MLCT or $\pi_{MN}$LCT?) are likely to be present. On the basis of comparison with the chlorides, the transitions labeled Band III in these compounds almost certainly contain LMCT transitions from the chloride ligands. If we assume that Band II does indeed contain $^1(nb_M, \pi_{MN})$, the separation between singlet and triplet transitions is $\sim$11 500 $cm^{-1}$ (see also the work of Gray et al. on $[Os(N)X_4]^-$).[15] This issue will be treated in detail in a future report.

**Radiative Deactivation.** Since direct population of the emissive excited state is observed in the absorption spectrum, the radiative decay rate may be calculated using the Strickler−Berg equation for spontaneous emission.[47,54] The Born−Oppenheimer approximation is assumed to be valid; electronic and vibrational components of the wave function are considered separable. Additionally, the nuclear configurations for the upper and lower states should be similar enough that the vibrational wave functions can be considered the same.[47] This formula was recast into experimentally measurable quantities, assuming Gaussian absorption and emission bands (eq 1)[55]

(53) Fowles, G. W.; Tidmarsh, D. J.; Walton, R. A. *Inorg. Chem.* **1969**, *8*, 631−638.
(54) Strickler, S. J.; Berg, R. A. *J. Chem. Phys.* **1962**, *37*, 814−822.
(55) Claude, J. P.; Williams, D. S.; Meyer, T. J. *J. Am. Chem. Soc.* **1996**, *118*, 9782−9783.

$$k_r = 3.05 \times 10^{-9} n^2 \langle \bar{\nu}_f^{-3} \rangle_{av}^{-1} \frac{\epsilon_{max} \Delta\bar{\nu}_{1/2}}{\bar{\nu}_{max}} \quad (1)$$

where $n$ is the refractive index of the medium, $\bar{\nu}_f \sim E_{em}$ or the emission maximum, and $\bar{\nu}_{max}$, $\Delta\bar{\nu}_{1/2}$, and $\epsilon_{max}$ are the energy maximum, the width at half-maximum and molar absorptivity of the corresponding absorption band, respectively. We have used eq 1 to calculate $k_r$ values and include them in Table 2. Calculated values overestimate the actual values by 1−2 orders of magnitude, despite the drastic approximations involved in this treatment. One expects $k_r$ to increase as $(E_{em})^3$, whereas this is clearly not the case. These rates can be compared with radiative rates for singlet and triplet transitions in aromatic compounds: $k_r$ (naphthalene fluorescence) = $1.8 \times 10^8$ s$^{-1}$, $k_r$ (anthracene fluorescence) = $6.4 \times 10^7$ s$^{-1}$ (benzene soln),[47] and $k_r$ (naphthalene phosphorescence) = $1.6 \times 10^{-2}$ s$^{-1}$.[49] Calculated rates for radiative deactivation using the Strickler−Berg treatment[54] are consistent with absorption and emission involving the same upper state (Table 2).[54]

There is in fact a correlation of $k_r$ with $(E_{em})^3$, but only if one considers the aryl compounds separately from the alkyl compounds, omitting **10** (Figure 4). Considering the Einstein relation from which eq 1 was derived, if $k_r \propto (E_{em})^3$, then the Einstein $B$ coefficient must be relatively invariant in the series. The discontinuity of the plot in Figure 4 further establishes that the aryl $\pi$ system significantly perturbs the electronic structure of the imido compounds by mixing with the Ta═N $\pi$-bond.[12,56] The trend breaks down for the cyanophenyl imido compound **10**, and we can only speculate that the electron withdrawing cyano group energetically removes the aryl $\pi$ system from conjugation with the Ta═N $\pi$ system, electronically making it a simple alkyl imido.

The reason for the scatter in Figure 4 from the alkyl imido group is unclear. We discern no trends as R or L is varied and postulate that this is experimental error introduced in the quantum yield measurements. While values obtained for these compounds are internally consistent and reproducible, the error in $k_r$ is probably still a significant contributor.

**Nonradiative Decay and Energy Gap Law Correlation.** A significant observation presented earlier[12] is the systematic variation in excited-state properties, most obviously emission energy and quantum yield, primarily as the imido substituent is changed. Specifically, the rate of nonradiative excited-state decay varies as a function of the emission energy.[12,57] An aryl substituent lowers the energy of the $^3(nb_M, \pi_{MN})$ transition, so an increase in $k_{nr}$ results. Energy gap behavior is observed for these compounds as a group, indicating that promoting and accepting vibrational modes are *relatively* invariant, but subtle deviations must exist. In other words, the vibrational characteristics which lead to nonradiative relaxation are relatively insensitive to the imido substituent despite differences in vibrational characteristics among them. There is some scatter in the alkyl region of Figure 5, however. Compounds with different alkyl substituents (i.e., not *aryl* substituents) but the same Lewis base have the same absorption and emission maxima (Table 2), e.g. **1c**, **2c**, **3c**, **4c**, etc. Thus there is no significant electronic impact at the Ta═N bond from the imido substituent; however, $\phi_{em}$ and $\tau$ vary noticeably among these compounds (Table 2), inconsistent with the gap law prediction that they will be essentially the same. However, there is still a

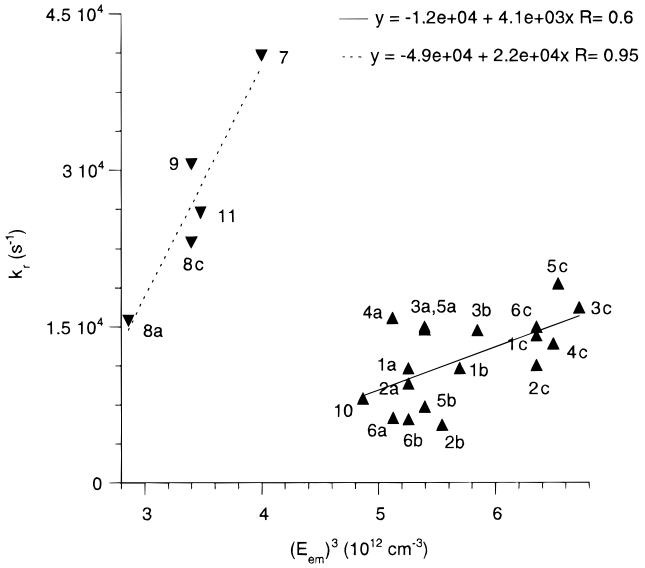


**Figure 4.** Plot of $k_r$ vs $(E_{em})^3$. The correlations correspond to least-squares fits of the alkyl and aryl imidos considered separately.

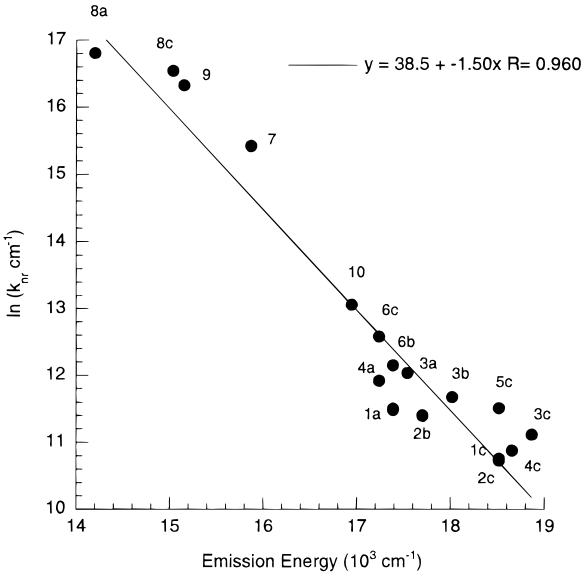


**Figure 5.** Plot of $\ln(k_{nr})$ vs $E_{em}$. The correlation is a least-squares fit to the data with a slope of $(650\ \text{cm}^{-1})^{-1}$.

reasonably good gap law correlation in Figure 5, suggesting that nonradiative decay processes in these imidos are relatively invariant. These issues will be treated in a later report.

**The Aryl Effect.** We are now in a position to elaborate on the aryl substituent effect on the basis of evidence for mixing of the aryl $\pi$ system with the metal−nitrogen $\pi$ system.[12,58] We rationalize the significant energy difference between R = alkyl, aryl to an interaction between the aryl and MN $\pi$ systems. Since both the aryl $\pi$ and $\pi_{MN}$ are filled, the result is an increase in the energy of the HOMO which is still $\pi_{MN}$ in character, but now contains aryl $\pi$. The energy of the $nb_M \leftarrow \pi_{MN}$ transition is thus significantly lowered, as depicted in Chart 3. From the absorption data, it is clear that the presence of an aryl substituent at nitrogen significantly lowers the energy of the lowest-energy absorption band. The calculations support this proposal as well, although calculated orbital energies do not. The HOMO of $[Ta(NPh)Cl_5]^{2-}$ shows a significant amount of aryl $\pi$ character,

(56) Maatta, E. A. *Inorg. Chem.* **1984**, *23*, 2560−2561.
(57) Kober, E. M.; Caspar, J. V.; Lumpkin, R. S.; Meyer, T. J. *J. Phys. Chem.* **1986**, *90*, 3722.
(58) Devore, D. D.; Lichtenhan, J. D.; Takusagawa, F.; Maatta, E. A. *J. Am. Chem. Soc.* **1987**, *109*, 7408−7416.

whereas there is little alkyl character in the $[Ta(N^tBu)Cl_5]^{2-}$ HOMO. In fact, a similar (small) amount of alkyl character is observed in $\pi_{//}$ of $[Ta(NPh)Cl_5]^{2-}$ and both $\pi_{//}$ and $\pi_{\perp}$ of $[Ta(N^tBu)Cl_5]^{2-}$ (Tables 4 and 5).

Maatta and co-workers reported a significant difference between the $^{51}V$ chemical shifts in $V(N^tBu)Cl_3$ and $V(Ntol)Cl_3$ ($\sim$300 ppm) while that of $VOCl_3$ is similar to the former.[58] This difference was attributed to significant destabilization of the V−N $\pi$-bonding orbital by overlap with the aryl $\pi$ system, thus lowering the energy of the HOMO−LUMO transition. The LUMO energy was predicted to be relatively invariant. In our scheme, a similar trend is rationalized, since the $d_{xy}$ (LUMO) should be unaffected by the nature of the imido substituent.

In terms of radiative electronic transitions, we can consider the variations in light of real electronic change in the bonding picture. There is a significant increase in the radiative transition probability for the aryl imidos compared to the alkyls (Figure 4, Table 2). If all imidos were in fact electronically identical, radiative decay rates for the aryl imidos should be much lower than is observed, according to eq 1. Therefore, while the aryl imidos must be electronically related to the alkyl imidos, there is a significant difference which increases the radiative rate and decreases the energy of the $^3(nb_M, \pi_{MN})$ state when R is aryl. This is attributed to significant overlap of the imido $\pi$-bond with the aromatic ring. Nonradiatively, however, the imido substituent seems to exhibit a comparatively small influence on excited-state dynamics. Thus we conclude that the "aryl effect" is primarily an electronic one and, furthermore, that these phenomena are general in multiply bonded systems with aryl substituents.

**Effect of Lewis Base Ligands on Excited-State Properties.** One can see that the effect of Lewis base ligands L in $Ta(NR)Cl_3L_2$ is significantly smaller than the effect of the imido alkyl substituent.[12,16] The $\pi$ interaction of dme, $Cl^-$, or py with the tantalum−nitrogen $\pi$-bond and $d_{xy}$ is weak,[45] and there will be only a small effect on excited-state properties from these ligands. In fact, there is only a small variation in emission energy upon changing L from an ether to a pyridine. Furthermore, the change is consistent with an energy gap effect rather than a significant electronic change; systematic changes in emission energy, $k_r$, and $k_{nr}$ are observed.

## Conclusions

These simple pseudooctahedral compounds are best considered 16-electron species; six $\sigma$-bonds from the ligands and two $\pi$-bonds from the imido nitrogen. The $\pi$-bonding is not as simple as is normally represented with aryl imidos due to significant interactions of the aryl and M═N $\pi$ systems. The simplistic picture shown in Chart 3 shows the two $\pi$-bonds formed (taking the M−N axis as $z$) by overlap of the Ta $d_{xz}$,$d_{yz}$ and the N $p_x$,$p_y$ which comprise the HOMO. The $d_{xy}$ is left nonbonding and is the LUMO. Next in energy is the Ta═N $\pi^*$. We believe that the lowest-energy absorptions in the compounds reported here occur into the $d_{xy}$ (nonbonding) orbital from the Ta═N $\pi$ bonding orbital and assign the transition as $nb \leftarrow \pi_{MN}$, rather than $\pi_{MN}^* \leftarrow \pi_{MN}$. At this point we have little firm evidence for the corresponding singlet transition, $^1(nb_M, \pi_{MN})$, in these compounds, although comparisons of the absorption spectra in Figure 1 seem to indicate the presence of this transition in Band II. Another (slim) possibility is that Band I in these compounds is a combination of both singlet and triplet transitions.

There are significant spectroscopic similarities between these compounds and $[Re(diimine)(CO)_3L]^+$.[42,43,59] Emission energies and emission quantum yields for the two classes are similar for the most part, with somewhat longer lifetimes being noted for the tantalum imido compounds. Alkyl substituent effects are observed in both systems. While in the Re compounds there is a good gap law correlation as the alkyl substituent is varied, the effect is more dramatic in the Ta imido systems, resulting from a pronounced electronic perturbation of the $\pi$ system. Another significant difference involves the absorption spectra. While in the imido compounds there is a well-resolved triplet absorption band which mirrors the emission band, in the rhenium compounds, the low-energy portion of the absorption spectrum is typically a long tail of overlapping transitions. The triplet absorption band is not resolved in the Re compounds.[42,43] These imido compounds represent a significant new class of luminescent inorganic chromophore which should prove a useful platform in development of future photochemical systems.

## Experimental Section

All sample manipulations were carried out in an Vacuum/Atmospheres nitrogen-filled drybox. General synthetic details may be found elsewhere, as well as preparative methods for all of the imido compounds referred to here.[6] 1,2-Dichloroethane used for spectroscopic experiments (spectroscopic grade from Burdick & Jackson) was distilled under argon from $CaH_2$ and then degassed and vacuum transferred from fresh $CaH_2$ prior to use. Absorption spectra were acquired on a Shimadzu PC-1000 UV−vis spectrophotometer in 1- and 10-mm path length cells. Emission and excitation spectra were recorded on a Spex Fluorolog DM-1B emission spectrophotometer. Emission spectra were corrected for PMT response and wavelength effects and were normalized for plotting.[47] Emission lifetimes were determined by monitoring emission on a Hamamatsu R928 photomultiplier tube interfaced to a LeCroy 9361 digital oscilloscope, with data reduction on a PC. Time-dependent response from the PMT was recorded on a digital oscilloscope and the data were fitted to a single-exponential decay using a Marquardt fitting algorithm. Excitation was provided by a PRA LN1000/LN107 nitrogen/dye laser combination. Lifetimes shorter than $\sim$50 ns were determined using a Spex $\tau$2 phase-shift fluorimeter with a fluorescein reference ($t$ = 4.05 ns).

Emission measurements were taken on the Fluorolog DM-1B with 2.5 mm slits in the emission monochromator. Emission data were corrected for spectrometer response prior to integration of the emission spectra. Emission quantum yields were determined using a standard ratiometric procedure[48]

$$\phi_U = \phi_S\left(\frac{I_U}{I_S}\right)\left(\frac{A_S}{A_U}\right)\left(\frac{\eta_S}{\eta_U}\right)^2 \qquad (2)$$

where $I_U$, $A_U$, and $\eta_U$ represent the integrated emission intensity, absorbance at the excitation wavelength, and the index of refraction of the solvent for the unknown and those quantities with the subscript S represent the standard. The emission standards used were $[Ru(bpy)_3][PF_6]_2$ in MeCN ($\phi_{em}$ = 0.012; aerated solution) and quinine sulfate in 1 N $H_2SO_4$ ($\phi_{em}$ = 0.51; aerated solution). Absorption data were acquired on the Shimadzu spectrophotometer with a blank solvent reference, and sample absorbances were less than 0.3 in all cases at the excitation wavelength.[48]

Absorption and emission spectra were converted into units of quanta per unit frequency interval ($dQ/d\bar{\nu}$ or $\epsilon(\bar{\nu})$ and $F(\bar{\nu})$, respectively) according to Parker and Rees.[60] The absorption spectra were then modified according to Birks and Dyson[47] into $\epsilon(\bar{\nu})/\bar{\nu}$ vs $\bar{\nu}$ (or $I(\bar{\nu})/\bar{\nu}$ vs $\bar{\nu}$ for excitation spectra). Luminescence spectra were converted into $F(\bar{\nu})/\bar{\nu}^3$, mirror image spectra were constructed as $F(2\bar{\nu}_0 - \bar{\nu})/(2\bar{\nu}_0 - \bar{\nu})^3$, and these were normalized and plotted as functions of $\bar{\nu}$.[47] The

(59) Caspar, J. V.; Meyer, T. J. *J. Phys. Chem.* **1983**, *87*, 952−957.
(60) Parker, C. A.; Rees, W. T. *Analyst* **1960**, *85*, 587−600.

values of $\bar{\nu}_0$ were determined by overlap of the modified absorption (or excitation) spectra with modified luminescence spectra.

Emission quenching experiments were carried out with 1 mM solutions of **10** in DCE containing anthracene in a concentration range 0.01−1 mM. Quenching rate constants were determined by plotting $k_{obs}$ vs [anthracene] and were linear at all concentrations of anthracene.

Electrochemical experiments were carried out in a dinitrogen-filled glovebox in a three-compartment cell in 0.1 M $[Bu_4N][PF_6]$/1,2-DCE. A Pt working and counter electrode were utilized, and Ag wire provided a pseudoreference. $Cp_2Fe$ was used as an internal reference. Data were acquired on a Radiometer PGP 201 potentiostat/galvanostat with output to an analog *x*/*y* chart recorder.

PM3 calculations were carried out on an Apple PowerMacintosh 8500/120 using MacSpartan Plus 1.1.6.[50,51] The molecules were constructed in the builder using the metrical parameters listed in the table. An MO calculation was then performed on the resulting structure. The resulting eigenvectors were then squared and normalized to a scale of 1 to compare percentage orbital character.

**Acknowledgment.** We are indebted to Professor John D. Petersen, Dean of Science, for generously providing access to his spectroscopy laboratory at Wayne State. D.S.W. thanks the National Science Foundation (Grant No. CHE-9632543) and the donors of the Petroleum Research Fund (#31361-G3), administered by the American Chemical Society, for generous support of this research. It is a pleasure to acknowledge Professor John F. Endicott for critical discussions and Professor Michael D. Hopkins for providing a preprint of reference 17 prior to publication.

**Supporting Information Available:** Complete output files and tables of percentage orbital contributions from the calculations on $[Ta(N^tBu)Cl_5]^-$ and $[Ta(NPh)Cl_5]^-$ (46 pages). Ordering information is given on any current masthead page.

IC9800740